Dynamics of Glyphosate Adsorption and Abiotic Transformations Pathways at Organo-Manganese Oxides Interface

Behrooz Azimzadeh and Carmen Enid Martínez*

Soil and Crop Sciences, School of Integrative Plant Science, College of Agriculture and Life Sciences, Cornell University, Ithaca, New York 14853, USA

*__Corresponding author__: Carmen Enid Martínez - Soil and Crop Sciences, School of Integrative Plant Science, College of Agriculture and Life Sciences, Cornell University, Ithaca, New York 14853, USA; Tel: +1 (607) 255-0895; Email: cem20@cornell.edu.

Keywords: Glyphosate, Organo-mineral association, Pathway selectivity, Catalytic oxidation degradation, Adsorption-desorption kinetics, Dissolved organic matter, Hausmannite, Birnessite

Synopsis: Protein-adsorbed Mn oxides hindered glyphosate retention and abiotic transformations, with AMPA pathway favored. Findings highlight regulatory role of sorbed organics on the functioning of active surfaces.

Abstract

Glyphosate, the most commonly used and widely detected herbicide worldwide, adsorbs and degrades on environmental surfaces, with natural organic matter playing a significant role in these processes. This study provides mechanistic and kinetic insights on how organo-mineral associations affect adsorption/desorption and abiotic oxidation of glyphosate. We use *in-situ* ATR-FTIR spectroscopy and microfluidic experiments coupled to LC-MS determination of glyphosate transformation by-products. A model protein (BSA) and Mn-oxide minerals (K-birnessite and hausmannite) are used. Results indicate the presence of protein adsorbed onto mineral surfaces (BSA-Mn oxide associations) favors the AMPA (+20%) over the glycine transformation pathway (-55%). The AMPA pathway is also favored in experiments conducted at circumneutral pH. The shift in pathway selectivity corresponds to changes in bonding of glyphosate with BSA-Mn oxide associations: we observe protein association enhances the contribution of the mononuclear monodentate conformation of glyphosate at the Mn oxide interface. In addition, protein association protects glyphosate from abiotic oxidation by diminishing Mn oxide catalytic activity (occupies surface active sites) and by forming organic-organic (i.e., glyphosate-protein) complexes. Furthermore, kinetic modeling shows protein association hinders the adsorption, desorption and transformation rate constants under circumneutral (pH 7.2) and acidic (pH 4.6) conditions. Since organo-mineral associations prevail in natural and engineer systems, the observed shifts in glyphosate transformation pathways that favor the formation of AMPA (a more toxic by-product) are relevant to human and ecosystem health.

Introduction

Glyphosate is used to control many weeds.[1] Due to its extensive use in agriculture, horticulture, forestry, and urban environments, glyphosate is frequently detected in soils, water bodies, food, and human fluids.[2-11] Additionally, transformation of laundry additives in wastewater (e.g., aminopolyphosphonates used as antiscalants) have been identified as a new source of glyphosate in European rivers.[12] Detection of glyphosate and its byproducts, specifically aminomethylphosphonic acid (AMPA), occurs despite their immobilization by microorganisms, abiotic degradation, or retention on metal oxides in soils.[13-19] Increased public concern regarding its potential toxicity and presence in the environment underscores the importance of research into its persistence and interactions within ecosystems.

Glyphosate primarily undergoes degradation through microbial activity, with additional contributions from abiotic mechanisms, which remain poorly understood.[20] Whether via biotic or abiotic mechanisms (**Scheme S1**), the degradation of glyphosate may occur through C(2)-N bond cleavage, which forms AMPA (AMPA pathway), a more toxic and resistant metabolite than glyphosate;[21-23] and/or through C(3)-P bond cleavage (sarcosine pathway), which yields innocuous products (i.e., sarcosine and then glycine).[16] A third degradation pathway (glycine pathway; C(3)-N bond cleavage) has also been proposed due to the inability to detect sarcosine.[24-26] The abiotic transformation and persistence of glyphosate and its byproducts vary significantly depending on environmental conditions. For example, the half-life (t1/2) of glyphosate ranges widely across soils ($t_{1/2} \approx 2$–174 days).[19, 25, 27, 28] This variation is strongly influenced by adsorption potential.[2, 27] Clay-rich soils with high organic matter content and low pH typically exhibit lower half-lives due to greater glyphosate adsorption. In a model water/Mn oxide catalytic system, which is the most commonly used system in studies of glyphosate

oxidation, glyphosate is notably unstable and degrades much faster ($t_{1/2} \approx 0.19 - 0.89$ hr).[26, 29, 30] Mn oxides are ubiquitous in soils and sediments, and highly redox-sensitive[31, 32] although fluctuation between oxic and anoxic conditions mainly impact Mn oxidation states in pore waters.[33, 34] Previous studies have shown that factors such as pH,[29] temperature,[16, 26, 35, 36] the presence of oxyanions and metals,[16, 36] redox conditions,[16] solid-to-solution ratio,[30, 37, 38] and initial concentration[29, 30] influence the catalytic activity of Mn oxides (predominantly birnessite) and the associated rates of transformation and pathway selectivity in the abiotic oxidation of glyphosate. Furthermore, different contribution of Mn valences (II, III and IV) impact the redox potential and reactivity of Mn oxide interfaces for transformation and stabilization of organic carbon.[31, 33, 34, 39, 40] Although the abiotic degradation of glyphosate by birnessite (δ-$Mn^{(III,IV)}O_2$) has been extensively studied[15, 16, 24, 26, 30, 35, 37, 38], there is no study demonstrating how Mn oxides with lower Mn valence states (i.e., hausmannite; $Mn_3^{(II,III)}O_4$) may contribute to adsorption and or degradation of glyphosate.

Dissolved organic matter (DOM), another critical component in environmentally relevant systems, can also affect the oxidation of organic contaminants via interactions in solution or after DOM adsorption onto mineral surfaces (i.e., after the formation of organo-mineral associations, OMAs). Previous studies have shown the oxidation kinetics of phenolic compounds by Mn oxides (birnessite) can change in the presence of soil or water derived DOM.[41-45] For example, Swenson *et al*.[41] showed that slower degradation rates result from competitive sorption between phenol and DOM coupled to reductive dissolution of birnessite. Conversely, they suggested that the cross-coupling reactions at the surface of DOM-MnO_2 association promote the degradation of phenolic compounds where enhanced DOM association led to formation of DOM-phenoxy radical species (via a one-electron-transfer between phenolic moieties of DOM and MnO_2).[41, 46]

In other case, Liu *et al*.[47] reported that a DNA macromolecule due to very high adsorption affinity mainly via its backbone phosphate, can block active sites of MnO_2 leading to suppressed oxidation of fluorescent peroxidase substrates. The inhibitory impact of organic association also is derived by surface passivation, where the pre-degradation of one organic constituent lower abiotic degradation of another which is associated to the dissolution/reduction mechanism.[48, 49] Proteinaceous materials derived from plant and microbial sources are a major active component of DOM in soils, sediments and aquatic environments.[50-54] Proteins have a high adsorption affinity to diverse mineral surfaces, such as iron (oxy)hydroxides,[55-58] layer aluminosilicates,[59] manganese oxides[48, 60-62] and other natural and engineered surfaces.[63-65] Generally, proteins unfold upon adsorption (e.g., loss of α-helices with conversion to turns), thus increasing the overall adhesive strength by the addition of hydrophobic interactions to electrostatic binding that leads to the formation of stable organo-mineral associations (OMAs).[56, 59, 62, 63, 66] Surface alteration by sorbed biomolecules may influence retention, transformation, and bioavailability of other organic constituents in natural systems.[14, 25, 48, 58, 67, 68] Although investigations of glyphosate's degradation on bare mineral surfaces are plentiful, the role of OMAs in governing the dynamics of both sorption-desorption and transformation of xenobiotics like glyphosate remains largely unexplored. Research utilizing heterogeneous organo-mineral associations will help us acquire a more realistic perspective of glyphosate's fate in the environment.

To address the identified knowledge gaps, we investigate the abiotic transformation pathways and adsorption-desorption mechanisms and kinetics of glyphosate with protein-Mn oxide associations. Experiments were conducted across minerals containing different Mn oxidation states (II, III, and IV) and under environmentally relevant pH conditions (4.6 and 7.2). This research employs *in-situ* time-resolved ATR-FTIR spectroscopy and microfluidic chamber

studies coupled with LC-MS and XPS analyses. Overall, Our findings reveal how glyphosate's interaction mechanism and its transformation pathways are tightly regulated by protein adsorption on Mn oxide minerals.

Material and Methods

Materials

Experiments were conducted using two Mn oxide minerals that differ in the Mn oxidation states (K-birnessite, δ-MnO_2 ; $(K^+)_x(Mn^{III}Mn^{IV})O_2 \cdot y(H_2O)$) and hausmannite ($(Mn^{II}Mn^{III}{}_2O_4)$. K-birnessite and hausmannite were synthesized as previously described[69, 70] with some modifications. Briefly, the synthesis of K-birnessite and hausmannite involves adding 2 M and 1 M KOH (Alfa Aesar, ≥ 99.98%) solutions to a 0.2 M $MnCl_2 \cdot 4H_2O$ (Alfa Aesar, ≥ 99.99%) solution at room temperature, and vigorously stirring with O_2 (flow ≈ 1.2 L min^{-1}) or without oxygenation, for ≈5hr, respectively. The precipitates were centrifuged and washed with DI water (18.2 MΩ·cm) to reach an electrical conductivity below 20 μS cm^{-1}. The purified pellets are then freeze-dried and stored in N_2-purged containers at 5 C° for further experiments. XRD diffractograms, TEM images, and physicochemical properties of synthesized Mn oxides are shown in **Figure S1** and **Table S1**, Supplementary Information (SI).

In-situ Time-resolved ATR-FTIR Adsorption-Desorption Experiments

In-situ time-resolved ATR-FTIR experiments were conducted to probe glyphosate adsorption-desorption dynamics and mechanisms on K-birnessite and hausmannite thin films, with and without pre-sorbed BSA protein, at pH 4.6 and 7.2. Experimental details can be found in our

previous work.[14, 68] Briefly, 5 µL of K-birnessite or hausmannite from 1.4 or 2.7 g L^{-1} suspensions (respectively) were drop-cast on the diamond internal reflective element (diamond IRE; area ≈ 7.1 mm^2) of the ATR accessory (Pike GladiATR™; Pike Technologies Madison, WI) and dried under a gentle stream of nitrogen gas. Based on the specific surface area of K-birnessite and hausmannite minerals (**Table S1**, SI), the Mn oxide films deposited on the diamond IRE had a similar total surface area (TSA ≈ 0.359 × 10^{-3} m^2). At this low TSA, the IR signals of expected byproducts (e.g., glycine and AMPA) were negligible compared to that of glyphosate adsorbed at the surfaces. Preliminary experiments were conducted to optimize the concentration of influent glyphosate (C_0) for *in-situ* ATR-FTIR experiments; a C_0 = 2 mM was used to obtain high spectral signal-to-noise ratio (>10). The adsorption step (i.e., Phase 1; duration = 37 min) was followed by a desorption step (i.e., Phase 2; duration = 31 min) using 10 mM KCl supporting electrolyte solution at pH 4.6 and 7.2. FTIR spectra were collected over a scan range of 4400 –150 cm^{-1} with an average 96 scans and resolution of 8 cm^{-1} (probing interval = 0.8 min). BSA-Mn oxide associations were synthesized by running 7.5 µM BSA protein over pre-conditioned Mn oxide films on the diamond IRE until equilibrium (see **Text S5** and **Figure S3** in SI for details). Experiments were repeated 3 – 4 times on freshly prepared films under identical conditions. All *in-situ* experiments were conducted under nitrogen gas purging and using an open-flow through system with a rate of 0.2 $mLmin^{-1}$, controlled by a peristaltic pump (Cole-Parmer, Vernon Hills, IL). ATR-FTIR spectra were collected on a Vertex 70 FTIR spectrometer (Bruker Corp., Billerica, MA). After collection, spectra received an atmospheric compensation, a nine-point Savitsky-Golay smoothing and baseline correction. All post-hoc manipulations were performed using OPUS v.7.2 software (Bruker Corp., Billerica, MA). Furthermore, the spectral features in the 1200 – 900 cm^{-1} range were deconvoluted in order to

156 determine the different interfacial configurations of adsorbed glyphosate through its phosphonate
157 group on Mn oxide and BSA-Mn oxide interfaces. Peak fitting of the spectra was carried out
158 using a second derivative deconvolution algorithm using PeakFit package v.4.12 (Systat
159 Software Inc., San Jose, CA). Details of this process can be found in our previous work.[14]

160 **Kinetic Modeling of Glyphosate Adsorption-Desorption in *in-situ* ATR-FTIR Experiments**

161 Adsorption and desorption kinetics of glyphosate on Mn oxide and BSA-Mn oxide interfaces
162 were estimated using the integral phosphonate frequency region (1200 to 910 cm $^{-1}$; ν(PO)). As
163 mentioned before, the IR signal of other PO-containing species (i.e., AMPA and orthophosphate)
164 in *in-situ* ATR-FTIR experiments were negligible, and the evolution of ν(PO) vibrational modes
165 were assumed to originate from adsorption and desorption of glyphosate only. All surface-
166 associated reactions were well described by the modified pseudo-first-order model[14], using Eq.
167 (1) for adsorption (Phase 1) and Eq. (2) for desorption (Phase 2):

$$A(\tilde{\nu})_t = A(\tilde{\nu})_{e,ads}\left(1 - e^{-k_a t}\right) \qquad for\ t \le t_e \tag{1}$$

$$A(\tilde{\nu})_t = A(\tilde{\nu})_{e,des}\, e^{-k_d (t - t_e)} \qquad for\ t > t_e \tag{2}$$

168 where, $A(\tilde{\nu})_t$ is the integral ν(PO) absorbance at time t (min), $A(\tilde{\nu})_e$ is the predicted integral ν(PO)
169 absorbance at adsorption or desorption equilibria, t_e is an arbitrary time (i.e., when Phase 1 was
170 switched to Phase 2: $t_e \approx 37$ min), and k_a and k_d are the adsorption and desorption rate constants
171 (min^{-1}), respectively.

172 **Glyphosate Transformation in Time-resolved Microfluidic Experiments**

Time-resolved microfluidic experiments were conducted with workflow similar to *in-situ* ATR-FTIR adsorption-desorption experiments to probe the dynamics of glyphosate's transformation and byproduct pathway selectivity on K-birnessite and hausmannite surfaces, with and without pre-sorbed BSA protein, at pH 4.6 and 7.2. A polycarbonate microfluidic chamber (w = 25 mm, l = 75 mm, and h = 0.24 mm) was fabricated for this study (**Figure S2A**). Mn oxide surfaces were prepared by drop-casting mineral suspensions on microscope slides (i.e., Mn oxide chips; Figure S2B; w = 16 mm, l = 66 mm; area ≈ 1,716 mm^2). The prepared Mn oxide chips had approximately the same total surface area (TSA ≈ 0.235 m^2). The experiments were initiated by conditioning of the Mn oxide chips by introducing a 10 mM KCl supporting electrolyte solution at pH 4.6 or 7.2 for 4 hr. Then, a glyphosate solution was introduced at a flow rate of 0.2 $mLmin^{-1}$ for 158 min (i.e., Phase 1). Phase 1 was followed by introducing the same background electrolyte solution (i.e., Phase 2, desorption; duration = 122 min). To study the impact of protein-Mn oxide associations on glyphosate transformations, BSA-Mn oxide associations were synthesized by introducing a 30 μM BSA solution over pre-conditioned Mn oxide chips for ≈ 2.5 hr. Then, to remove loosely bound protein molecules, the surface of BSA-Mn oxide chips was conditioned again by passing the same background electrolyte solution at corresponding pH values for ≈ 2 hr. All transformation experiments were performed using an input concentration, C_0, of 0.3 mM glyphosate in 10 mM KCl solution (I ≈ 10 mM) at pH 4.6 and 7.2. The effluents from the microfluidic chamber experiments were collected at 1.5 min time intervals using an automatic fraction collector in a deep-well plate for further analyses.

Effluent Analyses

194 The concentrations of glyphosate, AMPA, glycine and sarcosine were measured in the
195 effluents with a direct HILIC liquid chromatography mass spectroscopy (LC-MS) method.[71] The
196 instrumentation and details of the LC-MS methodology can be found in **Text S1, SI**. The
197 concentrations of orthophosphate[72] and ammonium[73] in the effluents were measured using
198 colorimetry. Total soluble Mn was measured using atomic absorption spectroscopy.

199 **Kinetic Modeling of Glyphosate Reactions on Mn Oxides in Microfluidic Experiments**

200 To understand the extent of the adsorption, transformation and desorption reactions, and solute
201 transport in the microfluidic system, the following mass balance equation, representing the ideal
202 plug-flow reactor (PFR) model, was applied:

$$[\text{Mass accumulation}]=[\text{In}]-[\text{Out}]+[\text{Generation}]-[\text{Consumption}] \quad (3)$$

203 We used the ideal PFR model where there is a steady flow ($Q_{in} = Q_{out} = 0.2$ mLmin^{-1}) with no
204 diffusion or dispersion across the boundaries. In Phase 1, the net input by advection was based
205 on the system's response to a "step" input, where a constant input concentration ($C_0 = 0.3$ mM)
206 was maintained over a period of time. In Phase 2, the system was evaluated with a "pulse" input,
207 where no input concentration ($C_0 = 0$ mM) was applied, and the effluent concentration gradually
208 decreased to zero according to the system's residence time distribution (τ). τ measured using a
209 Br^- tracer test, was estimated at ≈2.45 min for the used microfluidic chamber (**Figure S2C**, SI).
210 The "consumption" by reaction term includes adsorption and/or transformation reactions, and the
211 "generation" by reaction term results from the formation and/or desorption reactions. Glyphosate
212 (GP) adsorption, and its transformation and generation of byproducts in effluents may include

two parallel-consecutive reactions, as described in **Scheme 1.** The first reaction (i.e., adsorption of glyphosate) is reversible but the transformation reactions are irreversible.

Scheme 1. Proposed glyphosate adsorption (1) and transformation pathways (2) on Mn oxides.

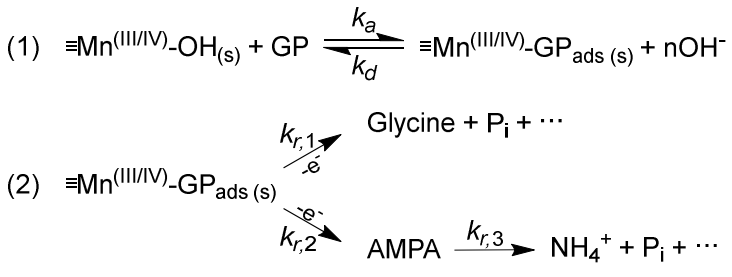

For the sake of simplicity, the intermediate species amino methyl phosphonic acid (AMPA) and its adsorption-desorption rate constants are not included in this scheme. Therefore, $k_{r,3}$ reflects the combined effects of adsorption-desorption and transformation of AMPA. Within this framework, the transformation rate expressions for glyphosate, glycine, AMPA, NH_4^+ and P_i can be written as, Eqs. 1 – 5:

$$rate_{\mathrm{GP}} = \frac{d[\mathrm{GP}]}{dt} = -k_a[\mathrm{GP}] + k_d[\mathrm{GP_{ads}}] \quad (1)$$

$$rate_{\mathrm{Glycine}} = \frac{d[\mathrm{Glycine}]}{dt} = k_{r,1}[\mathrm{GP_{ads}}] \quad (2)$$

$$rate_{\mathrm{AMPA}} = \frac{d[\mathrm{AMPA}]}{dt} = k_{r,2}[\mathrm{GP_{ads}}] - k_{r,3}[\mathrm{AMPA}] \quad (3)$$

$$rate_{\mathrm{NH_4^+}} = \frac{d[\mathrm{NH_4^+}]}{dt} = k_{r,3}[\mathrm{AMPA}] \quad (4)$$

$$rate_{\mathrm{P_i}} = \frac{d[P_i]}{dt} = k_{r,1}[\mathrm{GP_{ads}}] + k_{r,3}[\mathrm{AMPA}] \quad (5)$$

where, k_a and k_d are the adsorption and desorption rate constants (min^{-1}) of glyphosate, respectively. $k_{r,1}$ and $k_{r,2}$ are the transformation rate constants of glyphosate in the glycine and

AMPA pathways, respectively, and $k_{r,3}$ is the transformation rate constant of AMPA. The term "GP_{ads}" denotes adsorbed glyphosate that is an intermediate in the transformation reactions. The rate equation governing glyphosate adsorption processes is presented in Eq. 6:

$$rate_{GP_{ads}} = \frac{d[GP_{ads}]}{dt} = k_a[GP] - k_d[GP_{ads}] - \left(k_{r,1} + k_{r,2}\right)[GP_{ads}] \quad (6)$$

To solve Eqs. 1 to 5, a steady-state approximation for $d[GP]/dt$ can be applied, assuming that the system undergoes a catalytic reaction, where the adsorption reaction is very slow in comparison to transformation reactions of glyphosate: $k_{r,1}$ or $k_{r,2} >> k_a$. Consequently, there is no accumulation of adsorbed glyphosate, or it remains relatively constant throughout the reaction (i.e., $d[GP_{ads}]/dt \approx 0$). The detailed derivation of the rate constants is provided in the **Text S2**, SI.

The selectivity for the AMPA pathway, S_{AMPA}, can be expressed by Eq. 7:[74]

$$S_{AMPA} = \frac{[AMPA]}{[Glycine]} \times 100 \quad (7)$$

Transformation of small organic molecules, such as glyphosate, at Mn oxide surfaces can lead to dissolution of the Mn oxide.[16, 49, 75] Surface dissolution may be caused by adsorption-chelation or redox processes that result in the formation of highly soluble $Mn^{(II/III)}$ complexes (i.e., $Mn^{(II/III)}$-GP).[76]. For either chelation or reductive dissolution mechanisms to occur, glyphosate needs to form a coordinate bond with surface-associated Mn(II) or Mn(III) atoms[49, 75, 77] as shown in **Scheme 2**.

Scheme 2. Glyphosate-promoted dissolution reaction after or during transformation of glyphosate on Mn oxides.

$$\equiv Mn^{(II/III)}\text{-}(OH/P_i)_{(s)} + GP \underset{k_d}{\overset{k_a}{\rightleftharpoons}} \equiv Mn^{(II/III)}\text{-}GP_{ads\ (s)} + OH^-/P_{i\ (aq)} \xrightarrow{k_D} Mn^{(II/III)}\text{-}GP_{(aq)}$$

where k_D is the ligand-promoted dissolution rate constant (min^{-1}), inclusive of both chelation and/or reductive dissolution reactions. Mn oxide dissolution may proceed along with or after oxidation of glyphosate (**Scheme 2**) depending on the Mn valence state. We propose the following first-order rate expression for the formation of soluble $Mn^{(II/III)}$-GP complexes:

$$rate_{Mn^{(II/III)}\text{-GP}} = \frac{d[Mn^{(II/III)}\text{-GP}]}{dt} = k_D[GP_{ads}] \quad (8)$$

Derivatization of the dissolution rate constant is described in **Text S3**, SI.

Oxidation State Characterization for Surface-Associated Mn

Quantification of Mn oxide transformation using dissolved Mn as a metric may overlook reduced Mn on the solid phase or Mn that has re-oxidize on the mineral surface.[49] Therefore, X-ray photoelectron spectroscopy (XPS) data was obtained from the Mn oxide chips before and after microfluidic experiments to determine the contribution of Mn(II), Mn(III) and Mn(IV) by curve fitting of the high-resolution XPS Mn 3p spectra as described by Ilton *et al*.[39] See **Text S4**, SI for details on XPS instrumentation and measurement.

Results and Discussion

Glyphosate Adsorption-Desorption on BSA-Mn Oxide Associations: Mechanisms and Kinetics

The formation of BSA-Mn oxide associations is fully described in **Text S5**, SI. Briefly, ATR-FTIR spectral results indicate BSA protein adsorbs onto Mn oxides through its amide I, II and III bands, with additional peaks related to side-chain interactions (**Figure S3A**, SI). BSA adsorption

on Mn oxide is also associated with surface water loss. Adsorption of BSA is higher on hausmannite than on K-birnessite, and also higher at pH 4.6 than 7.2, influenced by pH-dependent electrostatic forces. No significant protein hydrolysis (i.e., break of C-N linkage) was observed, as no band shifts or signal loss were detected for amide II during BSA coating and stabilization (**Figure S3B**). Therefore, we do not expect any potential interference from BSA breakdown on the surface of Mn oxides in this study.

The (de)protonation of glyphosate significantly affects its interactions at water/solid interfaces.[78] The predominant glyphosate species (>98%) at pH 4.6 and 7.2 are the monoanion [$^{-}$OOCCH$_2$N^{+}H$_2$CH$_2$-HPO$_3^{-}$] and dianion [$^{-}$OOCCH$_2$N^{+}H$_2$CH$_2$-PO$_3^{2-}$], respectively (**Figure S4,** SI). Despite being a tridentate ligand, evidence increasingly suggests glyphosate's carboxylate and amine groups do not directly interact with goethite (i.e., do not form inner-sphere (IS) complexes).[14, 78-80] but form H-bonds (i.e., outer-sphere (OS) complexes) with other glyphosate molecules at the goethite interface and with organic molecules in OMAs (e.g., with polysaccharide in polysaccharide-goethite associations).[14, 68]

Representative *in-situ* ATR-FTIR spectra of glyphosate's retention dynamics at BSA-Mn oxide and Mn oxide interfaces highlight the progression of glyphosate adsorption and desorption through increases and decreases in intensity of the phosphonate (1200 – 900 cm^{-1}; $\nu(PO)$) and carboxylate-amine (1690 – 1515 cm^{-1}; $\nu(CAc)$) regions of the spectra (**Figure 1A**). Tentative peak assignments of adsorbed glyphosate at pH 4.6 and 7.2 are given in **Table S2**.

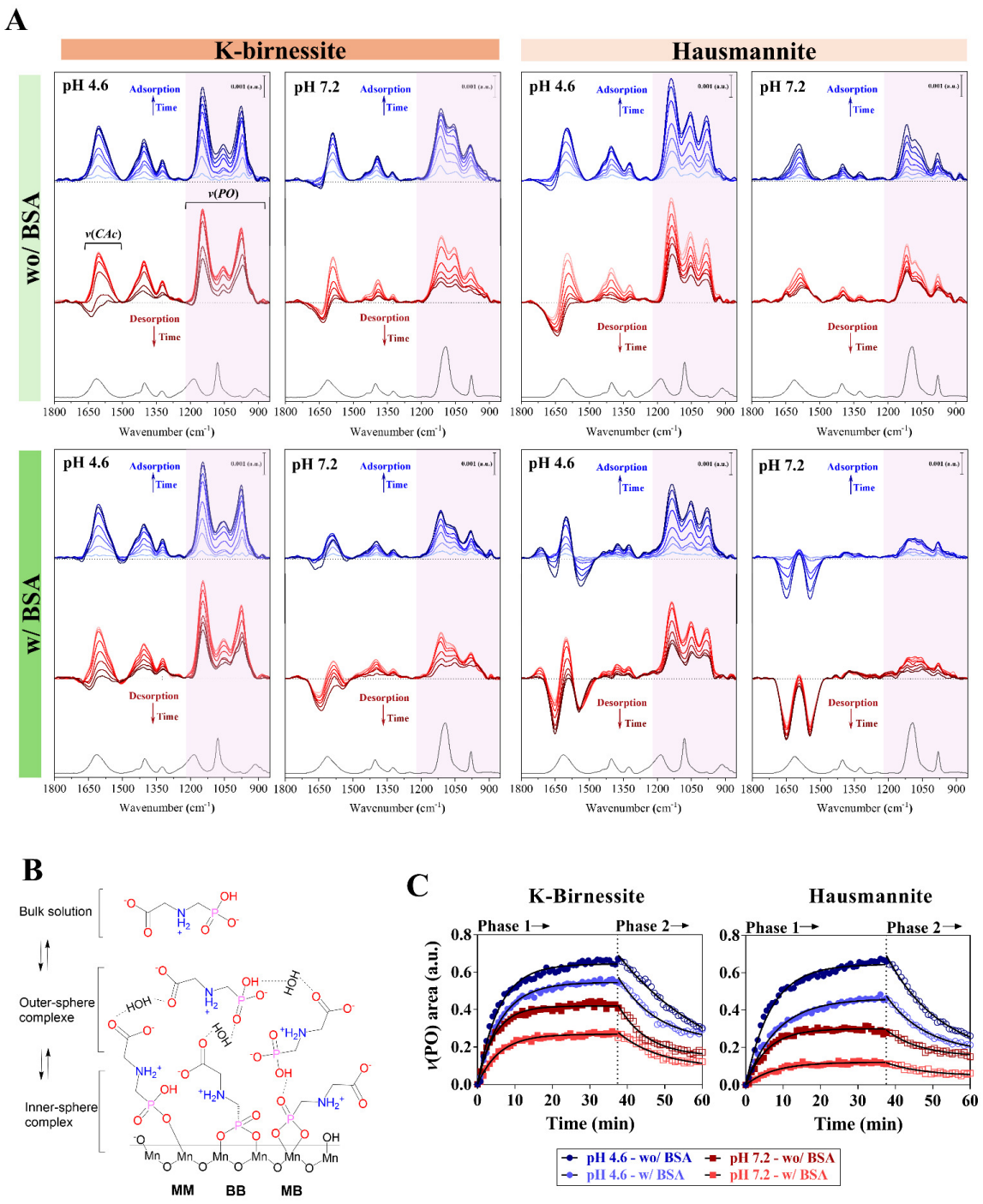

Figure 1. Glyphosate adsorption-desorption dynamics on Mn oxides at pH 4.6 and 7.2 with and without protein (BSA) association. (A) *In-situ* adsorption-desorption ATR-FTIR spectra. All spectra are on the same absorbance scale. Lighter and darker color spectra represent earlier and later time points, respectively (interval ≈ 2 – 4 min). Shaded area corresponds to vibrations (1200

– 900 cm^{-1}) in the interfacial phosphonate band region (B) Tentative interfacial outer- and inner-sphere complexes on Mn oxide, including mononuclear monodentate (MM), mononuclear bidentate (MB), and binuclear bidentate (MB). Dashed lines represent intermolecular H-bonding and electrostatic interactions. (C) PSO adsorption-desorption kinetics of the phosphonate *v*(*PO*) IR band region of glyphosate.

Asymmetric and symmetric stretching vibrational modes of the carboxylate group of sorbed glyphosate were subjected to downward shifts of 4 – 24 cm^{-1} on Mn oxides and BSA-Mn oxide associations whereas interfacial $\delta(NH_2^+)$ vibrational modes were shifted to lower energies by 11 – 29 cm^{-1}. Generally, hydrogen bonding lowers the frequency of stretching vibrations by reducing the restoring force, while increasing the frequency of bending vibrations by introducing an additional restoring force.[81] Therefore, glyphosate's amine groups do not contribute to H-bonding in interfacial complexes (**Figure 1B**). Although downward shifts were observed to be greater at pH 7.2 and in the presence of BSA, No specific trend was observed in interfacial carboxylate-amine bands of glyphosate adsorbed on K-birnessite and hausmannite. This highlights the fact that H-bonds do not from between glyphosate's carboxylate and amine groups and Mn oxides' hydroxyl groups, and that H-bonds mainly occur in OS complexes (**Figure 1B**). We observed that glyphosate and BSA molecules form a reversible guest-host association in bulk solution via noncovalent interactions (**Figure S5**). This organic-organic interaction can impact glyphosate adsorption by increasing surface mixing entropy and stabilized the interfacial repulsive force due to formed H-bonds within glyphosate-BSA-Mn oxide association.

The negative progress in the IR signal intensity at ~1650 and ~1540 cm^{-1} in BSA-Mn oxide associations, corresponding to the amide I and II bands, indicates protein loss during glyphosate adsorption and desorption (Figure 1A and S3B). Additionally, the reduction at ~1650 cm^{-1} in all

307 experiments is linked to the formation of inner-sphere (IS) complexes (i.e., P-O-Mn bonds;
308 reaction (1) in Scheme 2) via phosphonate groups. This process results in the loss of surface
309 hydroxyl groups (≡Mn-OH) due to ligand-exchange reactions.[40] IS complexes are identified by
310 the appearance of IR frequencies in the phosphonate region (1200 – 900 cm^{-1}; ν(PO)). As
311 illustrated in **Figure 1B**, the phosphonate groups of glyphosate can form various IS complex
312 configurations, including mononuclear monodentate (MM), mononuclear bidentate (MB), and
313 binuclear bidentate (BB). Peak assignments and fitting for the various P-O-Mn configurations
314 are detailed in **Figure S6** and **Table S2**. The relative absorbance of P-O-Mn vibrational modes
315 indicates that pH and protein associations influence the type of IS configuration glyphosate
316 forms or prefers (**Figures 1A** and **S6**). At pH 4.6, the simultaneous disappearance of the ν(POH)
317 band at 917 cm^{-1} and the emergence of peaks at ~980 and ~930 cm^{-1} signify the development of
318 bidentate BB and MB coordination modes, respectively (Table S2 and Figure S6). Additionally,
319 the appearance of a phosphonate stretching vibrational mode at ~1109 cm^{-1}, along with the
320 ν(P=O) band at ~1130 cm^{-1}, indicates the formation of an MM configuration[78] (**Figure S6**). This
321 MM configuration more likely occur in the presence of BSA association at pH 4.6 and under
322 both BSA-associated and non-associated conditions at pH 7.2. Overall, these results indicate
323 weaker retention and a higher likelihood of glyphosate release from BSA-Mn oxide surfaces.
324 Kinetic modeling of adsorption and desorption was conducted using the integral area of the
325 *ν*(PO) bands; both processes were well described by the PFO kinetic model (**Figure 1B**). The
326 estimated PFO parameters for adsorption and desorption (**Table 1**) indicate BSA association
327 hinders the rate (k_a) and extent (A_e) of adsorption, and slightly hinders the rate of desorption, k_d.
328 The presence of BSA association had a greater effect on hausmannite than on K-birnessite
329 adsorption-desorption kinetics. Furthermore, with BSA association the k_a values for each K-

birnessite and hausmannite become more similar at both pH (~0.16 – 0.17 and ~0.12 min^{-1}, respectively). This suggests BSA association is more important than pH in determining rate of adsorption. Further, the presence of BSA association primarily diminished the intensities of adsorbed glyphosate (15.2 – 28.5 %; $\Delta\nu(PO)_{ads}$) at all conditions (**Figure 1C and Table 1**) this reduction was greater at pH 7.2 (35.9 – 59.5 %) rather than pH 4.6 (15.2 – 28.5 %).

Table 1. Pseudo-first-order (PFO) adsorption and desorption kinetic parameters for the phosphonate ($\nu(PO)$) frequency region of glyphosate on Mn oxides and BSA-Mn oxide associations at pH 4.6 and 7.2.

Mn oxide	pH	BSA	k_a (min^{-1})	k_d (min^{-1})	A_e (a.u.)	$\Delta\nu(PO)_{ads}$ (%)[a]
K-birnessite	4.6	wo/	0.174	0.037	0.644	-
		w/	0.160	0.034	0.546	15.2
	7.2	wo/	0.216	0.044	0.420	-
		w/	0.172	0.041	0.269	35.9
Hausmannite	4.6	wo/	0.147	0.046	0.646	-
		w/	0.120	0.038	0.462	28.5
	7.2	wo/	0.173	0.051	0.301	-
		w/	0.123	0.043	0.122	59.5

[a] $\Delta\nu(PO)_{ads}=[(A_{e\ (wo/BSA)} - A_{e\ (w/BSA)}) / A_{e\ (wo/BSA)}] \times 100$

Glyphosate Oxidation on Mn oxides and BSA-Mn Oxide Associations

Breakthrough curves show the concentration of byproducts from glyphosate oxidation generally follow the order: phosphate > glycine > AMPA > ammonium, with similar trends but lower concentrations detected in experiments with hausmannite, and at pH 7.2 (**Figure 2A and S7 and Table S4**). NH_4^+ was not detected with hausmannite. These results indicate that glycine is the dominant byproduct from glyphosate oxidation (at least initially) although AMPA concentrations

increase with time suggesting favorability for the AMPA pathway at later times. BSA association significantly suppressed the formation of glycine on K-birnessite at pH 4.6 and 7.2 (**Figure 2B** and **Table S4**). Estimated rate constants (**Table 2**) for glyphosate oxidation through the glycine ($k_{r,1}$) and AMPA ($k_{r,2}$) pathways and AMPA degradation ($k_{r,3}$) suggests glycine formation occurs at the early stage of the transformation sequence, but the AMPA pathway is preferred at the late stage. This is in good agreement with pervious work[25, 26] where AMPA was found to be more resistant to degradation compared to glyphosate. Furthermore, our preliminary *in-situ* adsorption-desorption experiments confirm that AMPA can bind to the surface of K-birnessite via its phosphonate groups (**Figure S8**). Therefore, lower AMPA concentrations detected in effluents compared to glycine (**Figure 2B**), and low estimated $k_{r,3}$ values may include the combined effects of adsorption and degradation of AMPA.[26] The rate of transformations on Mn oxides follow the sequence: $k_{r,1} >> k_{r,2} > k_{r,3}$. Notably, K-birnessite was able to degrade glyphosate with faster rates than hausmannite ($k_{r,1}$ and $k_{r,2}$), especially at pH 7.2 **(Table 2**). BSA association enhanced all the transformation rate constants ($k_{r,1}$, $k_{r,2}$, and $k_{r,3}$), except at pH 7.2 for $k_{r,1}$ (birnessite and hausmannite) and for $k_{r,3}$ (birnessite).

Selectivity for the AMPA pathway, as indicated by S_{AMPA} (**Table 2**), increased in the presence of BSA on K-birnessite at pH 4.6 (0.43 to 0.78) and 7.2 (0.23 to 0.47). However, the presence of BSA on hausmannite did not have this effect, likely due to its greater standard reduction potential (E^0) that results in lower catalytic oxidation activity[82, 83] ($E^0_{\text{K-birnessite}} \approx 1.23$ V and $E^0_{\text{hausmannite}} \approx 1.83$ V).[84] With increasing pH, in the absence or presence of BSA, corresponding S_{AMPA} values decreased and less AMPA was measured in collected effluents while glycine remained the dominant byproduct (**Figure 2B** and **Table 2** and **S4**). Lasty, K-birnessite showed

increased selectivity for the AMPA pathway over hausmannite at corresponding experimental conditions.

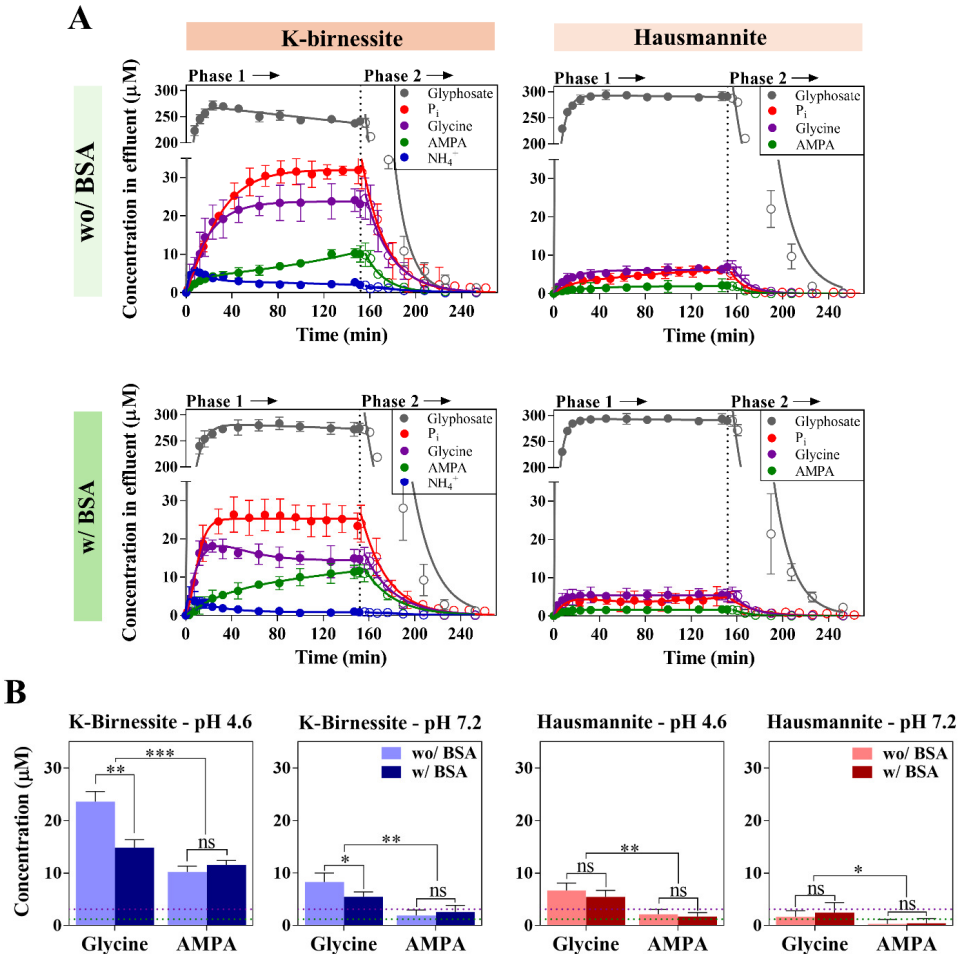

Figure 2. (A) Breakthrough curves of glyphosate and its byproducts in microfluidic chamber effluents. Shown are the results from experiments with K-birnessite and hausmannite at pH 4.6, with and without protein (BSA) association. Results from experiments at pH 7.2 can be found in the SI (**Figure S7**). (B) Concentration of glycine and AMPA in effluents at equilibrium (i.e., end of Phase 1; for details see **Table S4**). Symbol designations for the one-way ANOVA significant test results are: $p < 0.05$ (*), $p < 0.01$ (**), $p < 0.001$ (***), while "ns" denotes no significance. The purple and green dotted lines in (B) represent LoD for glycine (3.1 μM) and AMPA (1.2 μM).

Table 2. Rate constants for glyphosate transformation reactions and Mn oxide dissolution. The selectivity for AMPA pathway at equilibrium is also shown.

Mn oxide	pH	BSA	$k_{r,1}$ (min^{-1})	$k_{r,2}$ (min^{-1})	$k_{r,3}$ (min^{-1})	k_D (min^{-1})	S_{AMPA}
K-birnessite	4.6	wo/	0.49	0.04	0.02	0.006	0.43
		w/	0.98	0.43	0.03	0.012	0.78
	7.2	wo/	1.95	0.39	0.02	-	0.23
		w/	1.86	0.83	0.01	-	0.47
Hausmannite	4.6	wo/	0.35	0.02	-	0.058	0.32
		w/	0.82	0.31	-	0.302	0.31
	7.2	wo/	0.31	0.05	-	-	0.19
		w/	0.24	0.08	-	-	0.17

Integration of XPS results (Figure S5 and Table S4) with measured soluble Mn in the effluents reveals that dissolution of Mn oxide by glyphosate is predominately due to chelation dissolution mechanism at pH 4.6 (**Figure 3**). And this reaction is mainly governed by pH since no dissolved Mn was detected in collected effluents at pH 7.2. Reductive dissolution of Mn oxides, specially hausmannite, is a less significant mechanism, as the measured dissolved Mn does not show 1:1 proportional correlation with transformation byproducts (i.e., correspond to one-electron transfer reaction, **Scheme 1**). On the other hand, glyphosate and dissolved Mn in the effluents show 1:0.75 ratio which is respond to a chelation mechanism. In the presence of BSA association the extent of dissolution on Mn oxides diminishes and the glyphosate to dissolved Mn ratio is 1:0.55. As previously suggested, protein fragmentation is a catalyzed hydrolysis reaction and not an oxidative one[62] (as is the case with other organic molecules, such as glyphosate), in which Mn oxide do not reduce by BSA to Mn (II) or (III) and further loaded BSA blocks the active sites that subsequently protects the surface from being dissolved or reduced by glyphosate.[85, 86]

However, the dissolution rate constant (k_D) is greater at the presence of BSA association (**Table 2**). This result may be associated with mixing entropy effect.

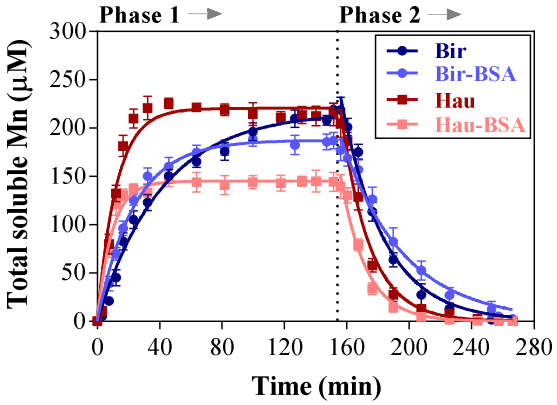

Figure 3. Breakthrough curves of total soluble Mn in effluents from K-birnessite (Bir) and hausmannite (Hau) experiments with and without protein (BSA) association at pH 4.6. Mn was not detected in effluents from experiments conducted at pH 7.2.

It has been suggested that soluble Mn (more likely Mn(II) species) can decrease the oxidative reactivity of glyphosate[16], and phenolic contaminants[41, 87] at the surface of Mn(IV) oxides. This occurs because (*i*) Mn(II) occupy active sites when sorbed, and (*ii*) Mn(II) can lower the redox potential of the system. As shown by quantitative XPS analysis (**Table S5**), increases in the Mn(II) fraction at the K-birnessite surface indicate reduced Mn(II) was re-adsorbed, as suggested by previous work.[41, 88, 89] This process may led to surface passivation.[88, 89] Furthermore, the adsorption of by-products such as P_i and AMPA may inhibit the reaction. These interactions suggest Mn(II) species, either in solution or at the surface, can modulate contaminant transformation, affecting the persistence and breakdown of agrochemicals like glyphosate in soil environments.

Glyphosate Bonding in Relation to Its Transformations

We observed that the glyphosate bonding configuration at the surface of Mn oxides significantly impacts subsequent C-N bond cleavage and transformation pathways. A positive strong correlation was identified between S_{AMPA} and the selectivity for mononuclear monodentate (MM) coordination complexes (i.e., S_{MM}, see **Text S6** for details) (**Figure 4**). The results indicate that the AMPA transformation pathway may govern by the type of bond glyphosate forms at Mn oxide surfaces over time. In particular, BSA association promoted the formation of MM complexes, which subsequently favored the AMPA pathway. The slopes of the lines in **Figure 4** reflect the rate of favorability for selective transformation of glyphosate via the AMPA pathway, with steeper slopes indicating greater favorability. Overall, the formation of AMPA was more favorable at the surface of K-birnessite compared to hausmannite. Additionally, surface modifications, including decreasing pH and the presence of BSA association, further increased the favorability (i.e., steeper slopes) for the AMPA pathway. In contrast, hausmannite exhibited a limited tendency for SAMPA transformation compared to K-birnessite at similar S_{MM} values. These results highlight how surface type and environmental conditions impact glyphosate bonding configurations at Mn oxide surfaces, dictating C-N bond cleavage and subsequent transformation pathways.

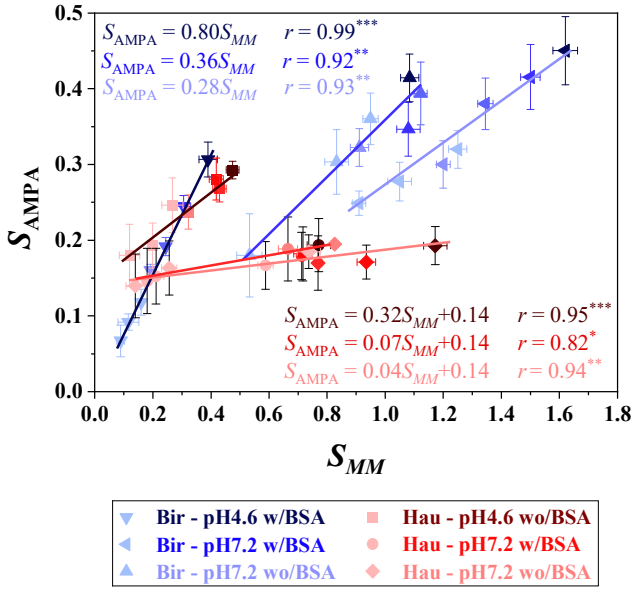

429

430 **Figure 4**. Correlation between selectivity for the AMPA pathway (S_{AMPA}) and mononuclear
431 monodentate (MM) coordination (S_{MM}) on K-birnessite (Bir) and hausmannite (Hau) at similar
432 adsorption times (t_{ads}: 0.8, 1.6, 2.4, 5.6, 8.8, 15.2, 31.2 min; represented by a color gradient). Data
433 include samples with MM coordination identified through spectroscopic analyses and AMPA
434 detection by LC-MS in effluents. Pearson correlation coefficients (r) and annotations for
435 associated p-values are provided.

436 **Environmental Implications**

437 While natural organic matter and Mn oxides are abundant[33, 90] and pivotal to contaminant
438 fate[41], the catalytic role of organo-mineral associations (e.g., protein-Mn oxide) in glyphosate
439 transformation remains underexplored. This study fills a critical gap, demonstrating the critical
440 role of organo-mineral associations in the abiotic transformation of glyphosate and enable us to
441 estimate glyphosate bioavailability and long-range transport in redox-sensitive environments. In
442 this study, we demonstrated that in the presence of protein association or with increasing pH,
443 both the transformation rate and capacity of glyphosate on BSA-Mn oxide associations diminish.

Additionally, a shift in glyphosate's abiotic transformation pathways may occur due to changes in its inner-sphere configurations. We demonstrated that the formation of monodentate complexes via phosphonate groups enhances the favorability of the AMPA pathway leading to increased production of AMPA, a toxic by-product, particularly at BSA-birnessite interface. Conversely, at lower pH or in the absence of BSA association, the formation of bidentate complexes is favored on Mn oxides, resulting in greater selectivity for the glycine pathway, which is a nutritional by-product. However, the glycine pathway is the predominant transformation pathway, while the sarcosine pathway, as in other studies, was not identified.[25, 26] Shifts in transformation pathways and their dynamics are critical for health and ecosystems, as DOM from various sources can enter natural systems, influencing both interfacial and organic-organic interactions of organic contaminants and nutrients. Overall, This research enhances understanding of organic contaminant behavior (e.g., glyphosate) at redox-active organo-mineral interfaces, where surface interactions govern retention, transport, bioavailability, and transformation in agricultural and engineered systems, offering insights for sustainable soil management and pollution mitigation strategies.

Supporting Information

Additional experimental and finding details, including Mn oxide characterization, microfluidic chamber with embedded Mn oxide chips, derivation of transformation and dissolution rate constants, instrumentation and experimental set-up for XPS and LC-MS, curve fitting and frequency assignments for glyphosate's $\nu(PO)$ bands, formation and *in-situ* ATR-FTIR spectra of BSA-Mn oxide complexes, speciation diagram of glyphosate and associated FTIR spectra of glyphosate at pH 4.6 and 7.2, complementary breakthrough curves of glyphosate and its

byproducts in effluents from microfluidic chamber at pH 7.2, ^{1}H STD-NMR spectra of BSA-glyphosate complex, AMPA *in-situ* adsorption-desorption spectra at the surface of K-birnessite at pH 4.6 and 7.2, and high resolution XPS Mn 3p spectra and curve fitting results for Mn oxides are provided in the supplementary information file.

Corresponding Author

Carmen Enid Martínez - Soil and Crop Sciences, School of Integrative Plant Science, College of Agriculture and Life Sciences, Cornell University, Ithaca, New York 14853, USA; Tel: +1 (607) 255-0895; Email: cem20@cornell.edu; https://orcid.org/0000-0001-8553-2118

Author

Behrooz Azimzadeh - Soil and Crop Sciences, School of Integrative Plant Science, College of Agriculture and Life Sciences, Cornell University, Ithaca, New York 14853, USA; https://orcid.org/0000-0001-9497-9843

Author Contributions

This study was conceptualized by C.E.M. and B.A. B.A. conducted the measurements, analysis, modeling, visualization, and wrote the first draft of the manuscript. All authors contributed to editing and reviewing the manuscript. Supervision, project administration, and funding acquisition were led by C.E.M.

Notes

The authors declare no competing financial interest.

Acknowledgements

Funding for this work was provided by the National Science Foundation (Award No. CHE-2003505) and the USDA National Institute of Food and Agriculture Hatch project (Accession No. 1020955). Graduate financial support for B.A. was provided by the Agriculture and Food Research Initiative (AFRI, Grant No. 2016-67019-25265/Project Accession No. 1009565) from the USDA National Institute of Food and Agriculture, the National Science Foundation (Award number CHE-2003505), and the College of Agriculture and Life Sciences at Cornell University. Partial research funding was also provided by a Graduate Research Grant from the Schmittau-Novak Small Grant Program from the School of Integrative Plant Science, Cornell University. This work utilized the shared instrumentation facility at the Cornell Center for Materials Research, as well as the NMR facility within the Department of Chemistry and Chemical Biology at Cornell University. Data from the microplate reader were obtained through the Cornell Institute of Biotechnology's BRC Imaging Facility. We would like to thank Robert Page for his assistance in fabricating the microfluidic reactor at the LASSP Professional Machine Shop, Cornell University. We also extend our gratitude to the anonymous reviewers for their invaluable feedback.

References

1. Franz, J. E.; Mao, M. K.; Sikorski, J. A., *Glyphosate: a unique global herbicide.* American Chemical Society: 1997.

2. Richards, B. K.; Pacenka, S.; Meyer, M. T.; Dietze, J. E.; Schatz, A. L.; Teuffer, K.; Aristilde, L.; Steenhuis, T. S. Antecedent and Post-Application Rain Events Trigger Glyphosate

Transport from Runoff-Prone Soils. *Environmental Science & Technology Letters* **2018,** *5* (5), 249-254.

3. Aparicio, V. C.; De Gerónimo, E.; Marino, D.; Primost, J.; Carriquiriborde, P.; Costa, J. L. Environmental fate of glyphosate and aminomethylphosphonic acid in surface waters and soil of agricultural basins. *Chemosphere* **2013,** *93* (9), 1866-1873.

4. Avigliano, E.; Schenone, N. F. Human health risk assessment and environmental distribution of trace elements, glyphosate, fecal coliform and total coliform in Atlantic Rainforest mountain rivers (South America). *Microchemical Journal* **2015,** *122*, 149-158.

5. Battaglin, W. A.; Meyer, M. T.; Kuivila, K. M.; Dietze, J. E. Glyphosate and its degradation product AMPA occur frequently and widely in US soils, surface water, groundwater, and precipitation. *JAWRA Journal of the American Water Resources Association* **2014,** *50* (2), 275-290.

6. Mahler, B. J.; Van Metre, P. C.; Burley, T. E.; Loftin, K. A.; Meyer, M. T.; Nowell, L. H. Similarities and differences in occurrence and temporal fluctuations in glyphosate and atrazine in small Midwestern streams (USA) during the 2013 growing season. *Science of the Total Environment* **2017,** *579*, 149-158.

7. Primost, J. E.; Marino, D. J.; Aparicio, V. C.; Costa, J. L.; Carriquiriborde, P. Glyphosate and AMPA,"pseudo-persistent" pollutants under real-world agricultural management practices in the Mesopotamic Pampas agroecosystem, Argentina. *Environmental Pollution* **2017,** *229*, 771-779.

8. Nunes, R. F. N.; Marciano, L. P. A.; Oliveira, G. S.; Cardoso, N. S.; Paula, F. B. d. A.; Sarpa, M.; Martins, I. Glyphosate contamination of drinking water and the occurrence of oxidative stress: Exposure assessment to rural Brazilian populations. *Environmental Toxicology and Pharmacology* **2024,** *108*, 104476.

9. Navarro, I.; de la Torre, A.; Sanz, P.; Abrantes, N.; Campos, I.; Alaoui, A.; Christ, F.; Alcon, F.; Contreras, J.; Glavan, M.; Pasković, I.; Pasković, M. P.; Nørgaard, T.; Mandrioli, D.; Sgargi, D.; Hofman, J.; Aparicio, V.; Baldi, I.; Bureau, M.; Vested, A.; Harkes, P.; Huerta-Lwanga, E.; Mol, H.; Geissen, V.; Silva, V.; Martínez, M. Á. Assessing pesticide residues occurrence and risks in water systems: A Pan-European and Argentina perspective. *Water Research* **2024,** *254*, 121419.

10. Gillezeau, C.; van Gerwen, M.; Shaffer, R. M.; Rana, I.; Zhang, L.; Sheppard, L.; Taioli, E. The evidence of human exposure to glyphosate: a review. *Environmental health : a global access science source* **2019,** *18* (1), 2-2.

11. Xu, J.; Smith, S.; Smith, G.; Wang, W.; Li, Y. Glyphosate contamination in grains and foods: An overview. *Food Control* **2019,** *106*, 106710.

12. Schwientek, M.; Rügner, H.; Haderlein, S. B.; Schulz, W.; Wimmer, B.; Engelbart, L.; Bieger, S.; Huhn, C. Glyphosate contamination in European rivers not from herbicide application? *Water Research* **2024,** *263*, 122140.

13. Zhao, H.; Tao, K.; Zhu, J.; Liu, S.; Gao, H.; Zhou, X. Bioremediation potential of glyphosate-degrading Pseudomonas spp. strains isolated from contaminated soil. *The Journal of general and applied microbiology* **2015,** *61* (5), 165-170.

14. Azimzadeh, B.; Martínez, C. E. Unraveling the role of polysaccharide-goethite associations on glyphosate' adsorption–desorption dynamics and binding mechanisms. *Journal of Colloid and Interface Science* **2024,** *653*, 1283-1292.

15. Ascolani Yael, J.; Fuhr, J.; Bocan, G.; Daza Millone, A.; Tognalli, N.; dos Santos Afonso, M.; Martiarena, M. Abiotic degradation of glyphosate into aminomethylphosphonic acid in the presence of metals. *Journal of agricultural and food chemistry* **2014,** *62* (40), 9651-9656.

16. Barrett, K. A.; McBride, M. B. Oxidative Degradation of Glyphosate and Aminomethylphosphonate by Manganese Oxide. *Environmental Science & Technology* **2005,** *39* (23), 9223-9228.

17. Okada, E.; Costa, J. L.; Bedmar, F. Adsorption and mobility of glyphosate in different soils under no-till and conventional tillage. *Geoderma* **2016,** *263*, 78-85.

18. Zhao, B.; Zhang, J.; Gong, J.; Zhang, H.; Zhang, C. Glyphosate mobility in soils by phosphate application: Laboratory column experiments. *Geoderma* **2009,** *149* (3), 290-297.

19. Al-Rajab, A. J.; Schiavon, M. Degradation of 14C-glyphosate and aminomethylphosphonic acid (AMPA) in three agricultural soils. *Journal of Environmental Sciences* **2010,** *22* (9), 1374-1380.

20. Zhan, H.; Feng, Y.; Fan, X.; Chen, S. Recent advances in glyphosate biodegradation. *Applied Microbiology and Biotechnology* **2018,** *102* (12), 5033-5043.

21. Eskenazi, B.; Gunier, R. B.; Rauch, S.; Kogut, K.; Perito, E. R.; Mendez, X.; Limbach, C.; Holland, N.; Bradman, A.; Harley, K. G.; Mills, P. J.; Mora, A. M. Association of Lifetime Exposure to Glyphosate and Aminomethylphosphonic Acid (AMPA) with Liver Inflammation and Metabolic Syndrome at Young Adulthood: Findings from the CHAMACOS Study. *Environmental Health Perspectives* **2023,** *131* (3), 037001.

22. Barreto, L. S.; Souza, T. L. d.; Morais, T. P. d.; Oliveira Ribeiro, C. A. d. Toxicity of glyphosate and aminomethylphosphonic acid (AMPA) to the early stages of development of Steindachneridion melanodermatum, an endangered endemic species of Southern Brazil. *Environmental Toxicology and Pharmacology* **2023,** *102*, 104234.

23. Folmar, L. C.; Sanders, H. O.; Julin, A. M. Toxicity of the herbicide glyphosate and several of its formulations to fish and aquatic invertebrates. *Archives of Environmental Contamination and Toxicology* **1979,** *8* (3), 269-278.

24. Li, H.; Wallace, A. F.; Sun, M.; Reardon, P.; Jaisi, D. P. Degradation of glyphosate by Mn-oxide may bypass sarcosine and form glycine directly after C–N bond cleavage. *Environmental science & technology* **2018,** *52* (3), 1109-1117.

580 25. Sun, M.; Li, H.; Jaisi, D. P. Degradation of glyphosate and bioavailability of phosphorus
581 derived from glyphosate in a soil-water system. *Water Research* **2019,** *163*, 114840.

582 26. Moller, S. R.; Wallace, A. F.; Zahir, R.; Quadery, A.; Jaisi, D. P. Effect of temperature on
583 the degradation of glyphosate by Mn-oxide: Products and pathways of degradation. *Journal of*
584 *Hazardous Materials* **2024,** *461*, 132467.

585 27. Bergström, L.; Börjesson, E.; Stenström, J. Laboratory and lysimeter studies of glyphosate
586 and aminomethylphosphonic acid in a sand and a clay soil. *Journal of Environmental Quality*
587 **2011,** *40* (1), 98-108.

588 28. Muskus, A. M.; Krauss, M.; Miltner, A.; Hamer, U.; Nowak, K. M. Degradation of
589 glyphosate in a Colombian soil is influenced by temperature, total organic carbon content and
590 pH. *Environmental Pollution* **2020,** *259*, 113767.

591 29. Manassero, A.; Passalia, C.; Negro, A. C.; Cassano, A. E.; Zalazar, C. S. Glyphosate
592 degradation in water employing the H2O2/UVC process. *Water research* **2010,** *44* (13), 3875-
593 3882.

594 30. Jaisi, D. P.; Li, H.; Wallace, A. F.; Paudel, P.; Sun, M.; Balakrishna, A.; Lerch, R. N.
595 Mechanisms of Bond Cleavage during Manganese Oxide and UV Degradation of Glyphosate:
596 Results from Phosphate Oxygen Isotopes and Molecular Simulations. *Journal of Agricultural*
597 *and Food Chemistry* **2016,** *64* (45), 8474-8482.

598 31. Post, J. E. Manganese oxide minerals: Crystal structures and economic and environmental
599 significance. *Proceedings of the National Academy of Sciences* **1999,** *96* (7), 3447-3454.

600 32. Namgung, S.; Chon, C.-M.; Lee, G. Formation of diverse Mn oxides: a review of
601 bio/geochemical processes of Mn oxidation. *Geosciences Journal* **2018,** *22* (2), 373-381.

602 33. Kravchenko, A. N.; Richardson, J. A.; Lee, J. H.; Guber, A. K. Distribution of Mn
603 Oxidation States in Grassland Soils and Their Relationships with Soil Pores. *Environmental*
604 *Science & Technology* **2022,** *56* (22), 16462-16472.

605 34. Wen, K.; Chadwick, O. A.; Vitousek, P. M.; Paulus, E. L.; Landrot, G.; Tappero, R. V.;
606 Kaszuba, J. P.; Luther, G. W.; Wang, Z.; Reinhart, B. J.; Zhu, M. Manganese Oxidation States
607 in Volcanic Soils across Annual Rainfall Gradients. *Environmental Science & Technology* **2023,**
608 *57* (1), 730-740.

609 35. Feng, D.; Malleret, L.; Soric, A.; Boutin, O. Kinetic study of glyphosate degradation in wet
610 air oxidation conditions. *Chemosphere* **2020,** *247*, 125930.

611 36. Ndjeri, M.; Pensel, A.; Peulon, S.; Haldys, V.; Desmazières, B.; Chaussé, A. Degradation
612 of glyphosate and AMPA (amino methylphosphonic acid) solutions by thin films of birnessite
613 electrodeposited: A new design of material for remediation processes? *Colloids and Surfaces A:*
614 *Physicochemical and Engineering Aspects* **2013,** *435*, 154-169.

37. Xiong, R.; Zhang, C.; Xiong, H.; Huang, S.; Li, J. Comparing the abiotic removal of glyphosate by β-MnO2 and δ-MnO2 colloids: Insights into kinetics and mechanisms. *Environmental Pollution* **2024,** *357*, 124432.

38. Paudel, P.; Negusse, A.; Jaisi, D. P. Birnessite-catalyzed degradation of glyphosate: A mechanistic study aided by kinetics batch studies and nmr spectroscopy. *Soil Science Society of America Journal* **2015,** *79* (3), 815-825.

39. Ilton, E. S.; Post, J. E.; Heaney, P. J.; Ling, F. T.; Kerisit, S. N. XPS determination of Mn oxidation states in Mn (hydr)oxides. *Applied Surface Science* **2016,** *366*, 475-485.

40. Brüggenwirth, L.; Behrens, R.; Schnee, L. S.; Sauheitl, L.; Mikutta, R.; Mikutta, C. Interactions of manganese oxides with natural dissolved organic matter: Implications for soil organic carbon cycling. *Geochimica et Cosmochimica Acta* **2024,** *366*, 182-200.

41. Swenson, J. T.; Ginder-Vogel, M.; Remucal, C. K. Influence of Divalent Cation Inhibition and Dissolved Organic Matter Enhancement on Phenol Oxidation Kinetics by Manganese Oxides. *Environmental Science & Technology* **2024,** *58* (5), 2479-2489.

42. Nguyen, H. V.-M.; Lee, D.-H.; Lee, H.-S.; Shin, H.-S. Investigating the different transformations of tetracycline using birnessite under different reaction conditions and various humic acids. *Environmental Pollution* **2023,** *339*, 122763.

43. Zhu, M.-X.; Wang, Z.; Xu, S.-H.; Li, T. Decolorization of methylene blue by δ-MnO2-coated montmorillonite complexes: Emphasizing redox reactivity of Mn-oxide coatings. *Journal of Hazardous Materials* **2010,** *181* (1), 57-64.

44. Kang, K.-H.; Dec, J.; Park, H.; Bollag, J.-M. Effect of phenolic mediators and humic acid on cyprodinil transformation in presence of birnessite. *Water Research* **2004,** *38* (11), 2737-2745.

45. Tong, F.; Gu, X.; Gu, C.; Xie, J.; Xie, X.; Jiang, B.; Wang, Y.; Ertunc, T.; Schäffer, A.; Ji, R. Stimulation of Tetrabromobisphenol A Binding to Soil Humic Substances by Birnessite and the Chemical Structure of the Bound Residues. *Environmental Science & Technology* **2016,** *50* (12), 6257-6266.

46. Song, Y.; Jiang, J.; Ma, J.; Zhou, Y.; von Gunten, U. Enhanced transformation of sulfonamide antibiotics by manganese(IV) oxide in the presence of model humic constituents. *Water Research* **2019,** *153*, 200-207.

47. Wang, L.; Huang, Z.; Liu, Y.; Wu, J.; Liu, J. Fluorescent DNA Probing Nanoscale MnO2: Adsorption, Dissolution by Thiol, and Nanozyme Activity. *Langmuir* **2018,** *34* (9), 3094-3101.

48. Reardon, P. N.; Walter, E. D.; Marean-Reardon, C. L.; Lawrence, C. W.; Kleber, M.; Washton, N. M. Carbohydrates protect protein against abiotic fragmentation by soil minerals. *Scientific Reports* **2018,** *8* (1), 813.

650 49. Li, H.; Reinhart, B.; Moller, S.; Herndon, E. Effects of C/Mn Ratios on the Sorption and
651 Oxidative Degradation of Small Organic Molecules on Mn-Oxides. *Environmental Science &*
652 *Technology* **2023,** *57* (1), 741-750.

653 50. Kleber, M.; Bourg, I. C.; Coward, E. K.; Hansel, C. M.; Myneni, S. C. B.; Nunan, N.
654 Dynamic interactions at the mineral–organic matter interface. *Nature Reviews Earth &*
655 *Environment* **2021,** *2* (6), 402-421.

656 51. Sutton, R.; Sposito, G. Molecular structure in soil humic substances: the new view.
657 *Environmental science & technology* **2005,** *39* (23), 9009-9015.

658 52. Ji, H.; Wang, H.; Wu, Z.; Wang, D.; Wang, X.; Fu, P.; Li, C.; Deng, W. Source,
659 composition and molecular diversity of dissolved and particulate organic matter varied with
660 riparian land use in tropical coastal headstreams. *Science of The Total Environment* **2024,** *908*,
661 168577.

662 53. Nebbioso, A.; Piccolo, A. Molecular characterization of dissolved organic matter (DOM): a
663 critical review. *Analytical and Bioanalytical Chemistry* **2013,** *405* (1), 109-124.

664 54. Ni, Z.; Wu, Y.; Ma, Y.; Li, Y.; Li, D.; Lin, W.; Wang, S.; Zhou, C. Spatial gradients and
665 molecular transformations of DOM, DON and DOS in human-impacted estuarine sediments.
666 *Environment International* **2024,** *185*, 108518.

667 55. Haynes, C. A.; Norde, W. Structures and Stabilities of Adsorbed Proteins. *Journal of Colloid*
668 *and Interface Science* **1995,** *169* (2), 313-328.

669 56. Liu, F.; Li, X.; Sheng, A.; Shang, J.; Wang, Z.; Liu, J. Kinetics and Mechanisms of
670 Protein Adsorption and Conformational Change on Hematite Particles. *Environmental Science &*
671 *Technology* **2019,** *53* (17), 10157-10165.

672 57. Ustunol, I. B.; Coward, E. K.; Quirk, E.; Grassian, V. H. Interaction of beta-lactoglobulin
673 and bovine serum albumin with iron oxide (α-Fe2O3) nanoparticles in the presence and absence
674 of pre-adsorbed phosphate. *Environmental Science: Nano* **2021,** *8* (10), 2811-2823.

675 58. Schmidt, M. P.; Martínez, C. E. Supramolecular association impacts biomolecule adsorption
676 onto goethite. *Environmental science & technology* **2018,** *52* (7), 4079-4089.

677 59. Schmidt, M. P.; Martínez, C. E. Kinetic and Conformational Insights of Protein Adsorption
678 onto Montmorillonite Revealed Using in Situ ATR-FTIR/2D-COS. *Langmuir* **2016,** *32* (31),
679 7719-7729.

680 60. Naidja, A.; Liu, C.; Huang, P. M. Formation of Protein–Birnessite Complex: XRD, FTIR,
681 and AFM Analysis. *Journal of Colloid and Interface Science* **2002,** *251* (1), 46-56.

682 61. Andersen, A.; Reardon, P. N.; Chacon, S. S.; Qafoku, N. P.; Washton, N. M.; Kleber, M.
683 Protein–Mineral Interactions: Molecular Dynamics Simulations Capture Importance of
684 Variations in Mineral Surface Composition and Structure. *Langmuir* **2016,** *32* (24), 6194-6209.

685 62. Reardon, P. N.; Chacon, S. S.; Walter, E. D.; Bowden, M. E.; Washton, N. M.; Kleber, M.
686 Abiotic protein fragmentation by manganese oxide: implications for a mechanism to supply soil
687 biota with oligopeptides. *Environmental science & technology* **2016,** *50* (7), 3486-3493.

688 63. Shang, W.; Nuffer, J. H.; Dordick, J. S.; Siegel, R. W. Unfolding of Ribonuclease A on
689 Silica Nanoparticle Surfaces. *Nano Letters* **2007,** *7* (7), 1991-1995.

690 64. Kim, J.; Doudrick, K. Emerging investigator series: protein adsorption and transformation
691 on catalytic and food-grade TiO2 nanoparticles in the presence of dissolved organic carbon.
692 *Environmental Science: Nano* **2019,** *6* (6), 1688-1703.

693 65. Limo, M. J.; Sola-Rabada, A.; Boix, E.; Thota, V.; Westcott, Z. C.; Puddu, V.; Perry, C.
694 C. Interactions between Metal Oxides and Biomolecules: from Fundamental Understanding to
695 Applications. *Chemical Reviews* **2018,** *118* (22), 11118-11193.

696 66. Schmidt, C. F.; Zimmermann, R. M.; Gaub, H. E. Multilayer adsorption of lysozyme on a
697 hydrophobic substrate. *Biophysical Journal* **1990,** *57* (3), 577-588.

698 67. Chacon, S. S.; Reardon, P. N.; Burgess, C. J.; Purvine, S.; Chu, R. K.; Clauss, T. R.;
699 Walter, E.; Myrold, D. D.; Washton, N.; Kleber, M. Mineral Surfaces as Agents of
700 Environmental Proteolysis: Mechanisms and Controls. *Environmental Science & Technology*
701 **2019,** *53* (6), 3018-3026.

702 68. Azimzadeh, B.; Nicholson, L. K.; Martínez, C. E. In the presence of the other: How
703 glyphosate and peptide molecules alter the dynamics of sorption on goethite. *Science of The*
704 *Total Environment* **2024,** *912*, 169264.

705 69. Chen, C.-C.; Golden, D.; Dixon, J. Transformation of synthetic birnessite to cryptomelane:
706 an electron microscopic study. *Clays and Clay Minerals* **1986,** *34* (5), 565-571.

707 70. Yeager, M. P.; Du, W.; Wang, Q.; Deskins, N. A.; Sullivan, M.; Bishop, B.; Su, D.; Xu,
708 W.; Senanayake, S. D.; Si, R. Pseudocapacitive Hausmannite Nanoparticles with (101) Facets:
709 Synthesis, Characterization, and Charge-Transfer Mechanism. *ChemSusChem* **2013,** *6* (10),
710 1983-1992.

711 71. Botero-Coy, A. M.; Ibáñez, M.; Sancho, J. V.; Hernández, F. Direct liquid
712 chromatography–tandem mass spectrometry determination of underivatized glyphosate in rice,
713 maize and soybean. *Journal of Chromatography A* **2013,** *1313*, 157-165.

714 72. Motomizu, S.; Wakimoto, T.; Tôei, K. Spectrophotometric determination of phosphate in
715 river waters with molybdate and malachite green. *Analyst* **1983,** *108* (1284), 361-367.

716 73. Rhine, E.; Mulvaney, R.; Pratt, E.; Sims, G. Improving the Berthelot reaction for
717 determining ammonium in soil extracts and water. *Soil Science Society of America Journal* **1998,**
718 *62* (2), 473-480.

719 74. van Santen, R. A.; Niemantsverdriet, J. W., *Chemical Kinetics and Catalysis*. 1st ed.;
720 Plenum Press: New York: 1995.

75. Stone, A. T.; Morgan, J. J. Reduction and dissolution of manganese (III) and manganese (IV) oxides by organics. 1. Reaction with hydroquinone. *Environmental Science & Technology* **1984,** *18* (6), 450-456.

76. Xu, Z.; Tsang, D. C. W. Mineral-mediated stability of organic carbon in soil and relevant interaction mechanisms. *Eco-Environment & Health* **2024,** *3* (1), 59-76.

77. Li, H.; Santos, F.; Butler, K.; Herndon, E. A Critical Review on the Multiple Roles of Manganese in Stabilizing and Destabilizing Soil Organic Matter. *Environmental Science & Technology* **2021,** *55* (18), 12136-12152.

78. Yan, W.; Jing, C. Molecular Insights into Glyphosate Adsorption to Goethite Gained from ATR-FTIR, Two-Dimensional Correlation Spectroscopy, and DFT Study. *Environmental science & technology* **2018,** *52* (4), 1946-1953.

79. Sheals, J.; Sjöberg, S.; Persson, P. Adsorption of glyphosate on goethite: molecular characterization of surface complexes. *Environmental science & technology* **2002,** *36* (14), 3090-3095.

80. Tribe, L.; Kwon, K. D.; Trout, C. C.; Kubicki, J. D. Molecular orbital theory study on surface complex structures of glyphosate on goethite: calculation of vibrational frequencies. *Environmental science & technology* **2006,** *40* (12), 3836-3841.

81. Colthup, N., *Introduction to infrared and Raman spectroscopy*. Elsevier: 2012.

82. Ukrainczyk, L.; McBride, M. B. Oxidation of phenol in acidic aqueous suspensions of manganese oxides. *Clays and Clay Minerals* **1992,** *40*, 157-166.

83. Stumm, W.; Morgan, J. J., *Aquatic chemistry: chemical equilibria and rates in natural waters*. John Wiley & Sons: 2013.

84. Bricker, O. Some stability relations in the system Mn-O2-H2O at 25 and one atmosphere total pressure. *American Mineralogist: Journal of Earth and Planetary Materials* **1965,** *50* (9), 1296-1354.

85. Liljeström, T.; Kontturi, K. S.; Durairaj, V.; Wester, N.; Tammelin, T.; Laurila, T.; Koskinen, J. Protein Adsorption and Its Effects on Electroanalytical Performance of Nanocellulose/Carbon Nanotube Composite Electrodes. *Biomacromolecules* **2023,** *24* (8), 3806-3818.

86. Harris, A. R.; Carter, P.; Cowan, R.; Wallace, G. G. Impact of protein fouling on the charge injection capacity, impedance, and effective electrode area of platinum electrodes for bionic devices. *ChemElectroChem* **2021,** *8* (6), 1078-1090.

87. Li, F.; Liu, C.; Liang, C.; Li, X.; Zhang, L. The oxidative degradation of 2-mercaptobenzothiazole at the interface of β-MnO2 and water. *Journal of Hazardous Materials* **2008,** *154* (1), 1098-1105.

88. Charbonnet, J. A.; Duan, Y.; van Genuchten, C. M.; Sedlak, D. L. Regenerated Manganese-Oxide Coated Sands: The Role of Mineral Phase in Organic Contaminant Reactivity. *Environmental Science & Technology* **2021,** *55* (8), 5282-5290.

89. Zhang, T.; Liu, L.; Tan, W.; Suib, S. L.; Qiu, G.; Liu, F. Photochemical Formation and Transformation of Birnessite: Effects of Cations on Micromorphology and Crystal Structure. *Environmental Science & Technology* **2018,** *52* (12), 6864-6871.

90. Zeng, C.; Yang, L.; Zhu, A.-X.; Rossiter, D. G.; Liu, J.; Liu, J.; Qin, C.; Wang, D. Mapping soil organic matter concentration at different scales using a mixed geographically weighted regression method. *Geoderma* **2016,** *281*, 69-82.